

One-Photon Photophysics and Two-Photon Absorption of 4-[9,9-Di-(2-ethylhexyl)-7-diphenylaminofluoren-2-yl]-2,2':6',2''-terpyridine and Their Platinum Chloride Complexes

Zhiqiang Ji,^[a] Yunjing Li,^[a] Timothy M. Pritchett,^[b] Nikolay S. Makarov,^[c] Joy E. Haley,^[d] Zhongjing Li,^[a] Mikhail Drobizhev,^[c] Aleksander Rebane,^[c] and Wenfang Sun*^[a]

Abstract: The synthesis, one-photon photophysics and two-photon absorption (2PA) of three dipolar D- π -A 4-[9,9-di(2-ethylhexyl)-7-diphenylaminofluoren-2-yl]-2,2':6',2''-terpyridine and their platinum chloride complexes with different linkers between the donor and acceptor are reported. All ligands exhibit ${}^1\pi,\pi^*$ transition in the UV and ${}^1\pi,\pi^*/{}^1\text{ICT}$ (intramolecular charge transfer) transition in the visible regions, while the complexes display a lower-energy ${}^1\pi,\pi^*/{}^1\text{CT}$ (charge trans-

fer) transition in the visible region in addition to the high-energy ${}^1\pi,\pi^*$ transitions. All ligands and the complexes are emissive at room temperature and 77 K, with the emitting excited state assigned as the mixed ${}^1\pi,\pi^*$ and ${}^1\text{CT}$ states at RT. Transient absorption from the ligands and the complexes were ob-

served. 2PA was investigated for all ligands and complexes. The two-photon absorption cross-sections (σ_2) of the complexes (600–2000 GM) measured by Z-scan experiment are much larger than those of their corresponding ligands measured by the two-photon induced fluorescence method. The ligand and the complex with the ethynylene linker show much stronger 2PA than those with the vinylene linker.

Keywords: luminescence • nonlinear optics • photophysics • platinum • two-photon absorption

Introduction

Two-photon absorbing (2PA) materials have aroused great attention in recent years, because of their potential applications in laser energy compression,^[1] 3D-microfabrication,^[2] two-photon microscopy,^[3] and two-photon photodynamic therapy.^[4] To date, the most widely investigated two-photon absorbing materials are small organic molecules possessing the structure motifs of dipolar donor- π -acceptor (donor and

acceptor refer to electron donor and electron acceptor, respectively),^[5] quadrupolar donor- π -donor,^[6] acceptor- π -acceptor,^[7] octupoles,^[8] multi-annulene,^[9] porphyrins,^[10] and TPA oligomers and polymers.^[11] Studies on the structure-property correlation of dipolar donor- π -acceptor compounds revealed that increased intramolecular charge transfer (ICT) could enhance the 2PA cross-section (σ_2), that is, the conjugation length and strength of donor and acceptor influence the σ_2 value.^[12]

Compared to the 2PA studies on organic compounds and dendrimers, relatively little work has been done on organometallic complexes as 2PA materials. Octupolar iron(II) and ruthenium(II) tris(quarterpyridinium) complexes that show weak to moderate 2PA were studied theoretically and by Z-scan experiment.^[13] Zinc phthalocyanines were studied using femtosecond fluorescence-based method, and the σ_2 values up to 400 GM ($1 \text{ GM} = 10^{-50} \text{ cm}^4 \text{ s photon}^{-1} \text{ molecule}^{-1}$) were observed.^[14] Much larger σ_2 values up to 17 000 GM were observed in zinc-porphyrin dimers.^[15] Pseudooctahedral Schiff base Zn^{II} and Cu^{I} complexes showed enhanced 2PA after metal coordination.^[16] There are several examples of platinum acetylide monomers and oligomers exhibiting 2PA in the visible to the near-IR region.^[17] However, except for the Schiff base Zn^{II} and Cu^{I} complexes that exhibit exceptionally large σ_2 values, the σ_2 values reported for these complexes have been quite small to moderate. The largest σ_2 value reported for platinum acetylide complexes is only 780 GM^[17c] to date. In addition, the photo-instability of

[a] Dr. Z. Ji, Dr. Y. Li, Z. Li, Dr. W. Sun
Department of Chemistry and Biochemistry
North Dakota State University, Fargo, ND 58108-6050 (USA)
Fax: (+1) 701-231-8831
E-mail: Wenfang.Sun@ndsu.edu

[b] Dr. T. M. Pritchett
US Army Research Laboratory, AMSRD-SE-EM
2800 Powder Mill Road, Adelphi, MD 20783-1197 (USA)

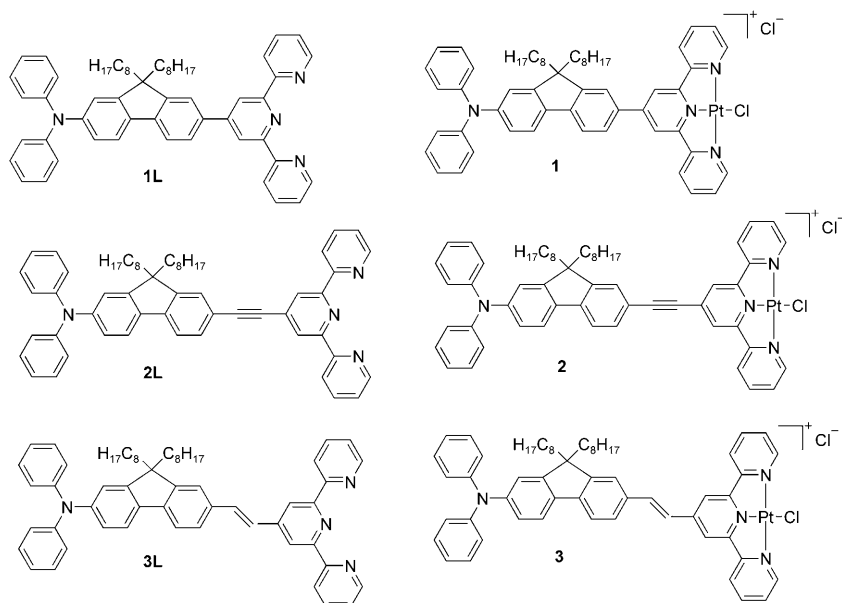
[c] N. S. Makarov, Dr. M. Drobizhev, Dr. A. Rebane
Department of Physics, Montana State University
Boltzmann, MT 59717 (USA)

[d] Dr. J. E. Haley
Materials and Manufacturing Directorate
Air Force Research Laboratory
Wright Patterson Air Force Base, Dayton, OH 45433 (USA)
and
UES, Inc., Dayton, OH 45432 (USA)

Supporting information for this article is available on the WWW under <http://dx.doi.org/10.1002/chem.201001449>.

these platinum acetylide complexes would prevent their potential applications for photonic devices.

To enhance the two-photon absorption of the platinum complexes and increase their photo-stability, in this work we designed and synthesized three dipolar ligands containing terpyridine component and their platinum chloride complexes (structures shown in Scheme 1). These ligands possess



Scheme 1. Chemical structure of the target molecules.

an unsymmetrical D- π -A geometry with a diphenylamino group as the electron donor, fluorenyl as the π -bridge, and terpyridine as the electron acceptor. They differ from each other in the connection pattern between the fluorenyl and the terpyridine components. All ligands and platinum complexes are expected to exhibit strong intramolecular charge transfer that could possibly lead to strong two-photon absorption. Systematic photophysical studies of all ligands and complexes are carried out to understand their excited-state properties. Wavelength dispersion of the two-photon absorption of the ligands and the platinum complexes is also studied via two-photon induced upconverted fluorescence and Z-scan techniques.

Results and Discussion

Synthesis: The synthetic schemes for the ligands and their corresponding platinum complexes are shown in Scheme 2. All ligands were synthesized from the same starting material, that is, 2-bromo-9,9-di(2-ethylhexyl)-7-diphenylamino-fluorene (**8**).^[18] Successive treatment of compound **8** with BuLi and 2-isopropoxy-4,4,5,5-tetramethyl-1,3,2-dioxaborolane gave the corresponding boronic ester **9**. Under Suzuki coupling reaction conditions, compound **9** reacted with 4'-

bromo-2,2':6',2''-terpyridine in the presence of K₂CO₃ to give ligand **1L** at a 67% yield. Reaction of **8** with 2-methyl-3-butyn-2-ol in the presence of palladium(0) catalyst and CuI gave compound **10** at a 40% yield. Deprotection of **10** yielded compound **11**. Reaction of **11** with 4'-(trifluoromethylsulfonyl)-2,2':6',2''-terpyridine via the Sonogashira coupling reaction gave ligand **2L** at a 75% yield. Ligand **3L** was synthesized by Heck reaction of compound **12** with compound **8** at a 78% yield. The platinum terpyridyl complexes **1–3** were synthesized by reaction of the corresponding ligand with [Pt(dmsO)₂Cl₂] in CHCl₃. Pure complexes were obtained by recrystallization in CH₂Cl₂ and hexane in 47–65% yield. All complexes were characterized by ¹H NMR spectroscopy, HRMS, and elemental analysis.

Electronic absorption: The electronic absorption spectra of **1L–3L** in CH₂Cl₂ at a concentration of 1 × 10⁻⁵ mol L⁻¹ are shown in Figure 1 and the molar extinction coefficients are summarized in Table 1. Compounds **1L–3L** all exhibit

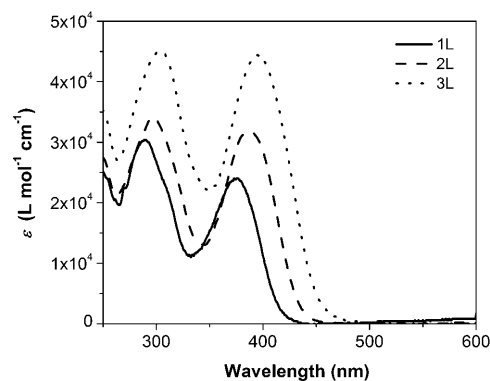
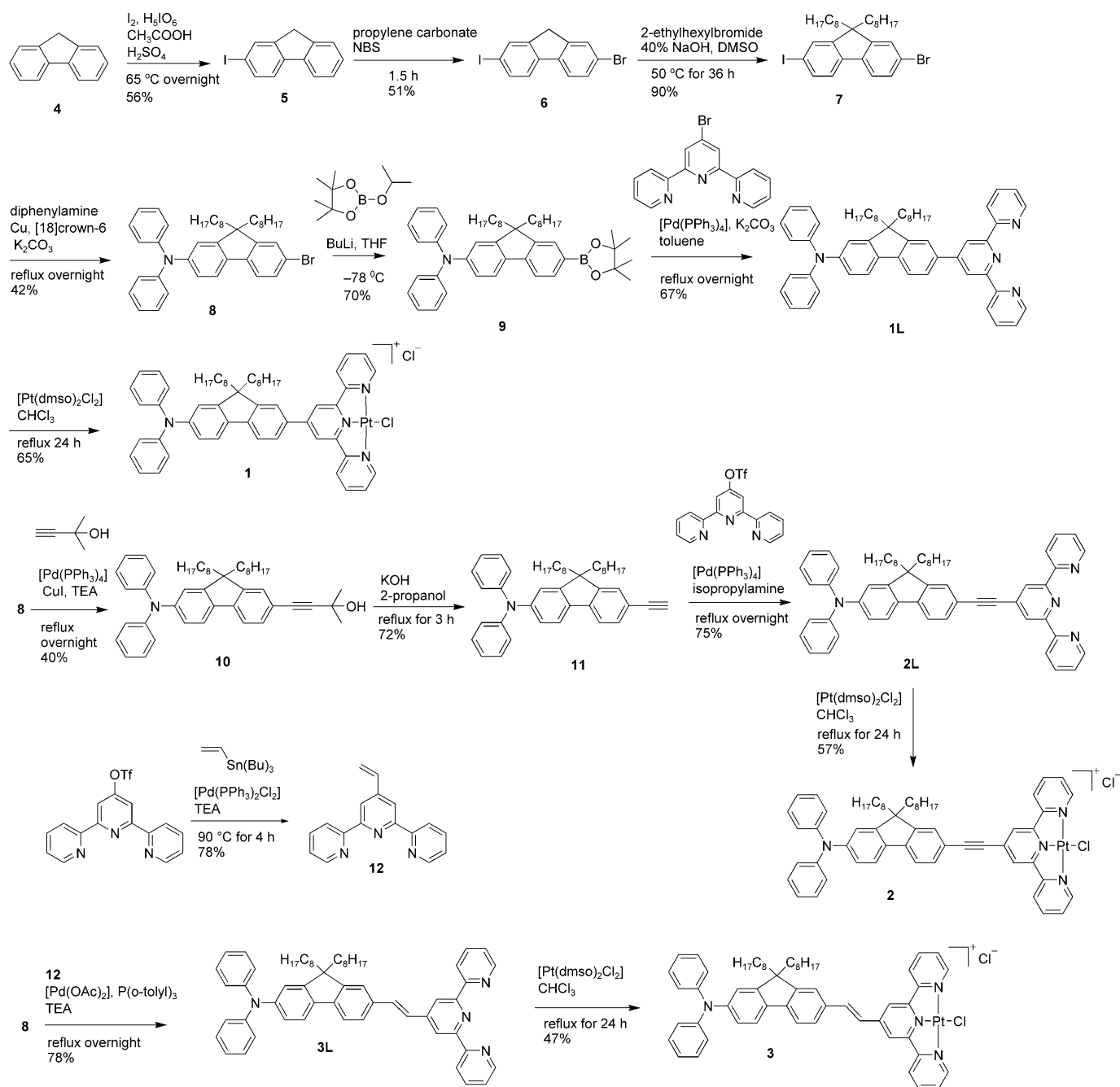


Figure 1. UV/Vis absorption spectra of **1L–3L** in CH₂Cl₂ at a concentration of 1 × 10⁻⁵ mol L⁻¹.

intense absorption in the UV and blue regions, which can be assigned as ¹ π,π^* and ¹ $\pi,\pi^*/\text{ICT}$ (intramolecular charge transfer) transitions, respectively. It is obvious that going from **1L** to **3L**, the energies of the absorption bands decrease, accompanied by an increase of the molar extinction coefficients. This trend could be attributed to the enhanced electronic coupling between the diphenylaminofluorene component and the terpyridine component, which results in the more extended π -conjugation and bathochromic shift of

Scheme 2. Synthetic route for **1L–3L** and **1–3**.Table 1. Electronic absorption and emission data for **1L–3L** and **1–3**.

	λ_{abs} [nm] (ϵ [$10^4 \text{ L mol}^{-1} \text{ cm}^{-1}$]) ^[a]	λ_{em} [nm] (τ) RT	Φ_{em} RT	λ_{em} [nm] (τ [μs]) 77 K
1L	290 (2.96), 376 (2.32)	484 (12 ns (26%), 102 ns (74%)) ^[b]	0.59 ^[d]	522, 569 ^[f]
2L	297 (3.48), 387 (3.16)	505 (12 ns (23%), 91 ns (76%)) ^[b]	0.70 ^[d]	582 ^[f]
3L	304 (4.08), 394 (4.44)	526 (33 ns (41%), 112 ns (59%)) ^[b]	0.42 ^[d]	594 ^[f]
1	284 (4.03), 334 (3.63), 471 (1.75)	515 (48 ps (29%), 2241 ps (71%)) ^[c]	0.00047 ^[e]	566 (119) ^[g]
2	283 (3.64), 338 (3.49), 361 (3.63), 466 (2.06)	486 (86 ps (2%), 3686 ps (98%)) ^[c]	0.00035 ^[e]	602 (88) ^[g]
3	284 (4.16), 338 (3.55), 365 (3.61), 492 (3.04)	532 (150 ps (8%), 2976 ps (92%)) ^[c]	0.00019 ^[e]	644 (22) ^[g]

[a] Electronic absorption band maxima and molar extinction coefficients in CH_2Cl_2 for **1L–3L**, and in CH_3CN for **1–3**, $c \approx 1 \times 10^{-5} \text{ mol L}^{-1}$. [b] Room temperature emission band maxima and decay lifetimes measured at a concentration of $1 \times 10^{-5} \text{ mol L}^{-1}$. [c] The emission band maxima and decay lifetimes measured in CH_3CN solutions. $\lambda_{\text{ex}} = 375 \text{ nm}$. [d] Emission quantum yield measured in CH_2Cl_2 solutions with $A_{350} = 0.1$. [e] Emission quantum yield measured at $\lambda_{\text{ex}} = 436 \text{ nm}$ with $A_{436} = 0.1$ in CH_3CN solution. $[\text{Ru}(\text{bpy})_3]\text{Cl}_2$ was used as the reference. [f] The emission band maxima at 77 K measured with 10 equivalents of CH_3I in 4:1 $\text{CH}_3\text{CH}_2\text{OH}/\text{CH}_3\text{OH}$ glassy solution, $c \approx 1 \times 10^{-5} \text{ mol L}^{-1}$. [g] The emission band maxima and decay lifetimes at 77 K measured in BuCN glassy solution, $c \approx 1 \times 10^{-5} \text{ mol L}^{-1}$. $\lambda_{\text{ex}} = 355 \text{ nm}$.

the absorption bands. The assignment of ${}^1\pi,\pi^*$ transitions to these absorption bands is supported by the large extinction coefficients of these bands and by the solvent-dependency study. As exemplified in Supporting Information Figure S1 for **1L**, minor solvent effect was observed, which is consistent with the ${}^1\pi,\pi^*$ character. The possible mixture of the ${}^1\text{ICT}$ character into the blue absorption band could be rationalized by the electron-donating ability of the diphenylamino substituent and the electron-withdrawing ability of the terpyridine component. It is further supported by the acid-titration study that will be discussed in the following paragraph, in which the increased electron-withdrawing ability of the protonated terpyridine causes a red-shift of the ${}^1\text{ICT}$ band, whereas the ${}^1\pi,\pi^*$ transition remains the same energy. Similar phenomenon was observed for **2L** and **3L**.

Because diphenylamino group is an electron-donating group and terpyridine motif would become a stronger electron-withdrawing group upon protonation, therefore, stronger and red-shifted intramolecular charge transfer (ICT) is anticipated to occur in acidic solution. To verify this, titration of **1L–3L** with *p*-TsOH was carried out. As exemplified in Figure 2 for **3L**, upon addition of *p*-TsOH, the absorption band at about 394 nm decreases, accompanied by the increase of a new absorption band at about 481 nm. These changes could be attributed to the protonation of the nitrogens in terpyridine. The resultant positive charges facilitate electron transfer from the electron-rich diphenylamino

group to the electron-deficient protonated terpyridine motif, which increases the degree of intramolecular charge transfer (${}^1\text{ICT}$) transition and bathochromically shifts the ${}^1\text{ICT}$ band. In this case, the ${}^1\pi,\pi^*$ transition and the ${}^1\text{ICT}$ transition are separated, which results in the decrease of the original ${}^1\pi,\pi^*/{}^1\text{ICT}$ absorption band at 394 nm. The charge transfer nature of the new absorption band at about 481 nm is evident from the negative solvatochromic effect due to the more polar charge-separated ground-state and the less polar excited state after charge transfer. As shown in Figure 2b for the protonated ligand **3L**, the low-energy absorption band is blue-shifted in more polar solvents, such as in MeOH and CH_3CN , compared to those in less polar solvents, which is a characteristic of a more polar charge-separated ground state. Similar phenomena were observed for **1L** and **2L**.

The electronic absorption spectra of platinum complexes **1**, **2**, and **3** were measured in CH_3CN solutions. As shown in Figure 3 and summarized in Table 1, these complexes exhibit

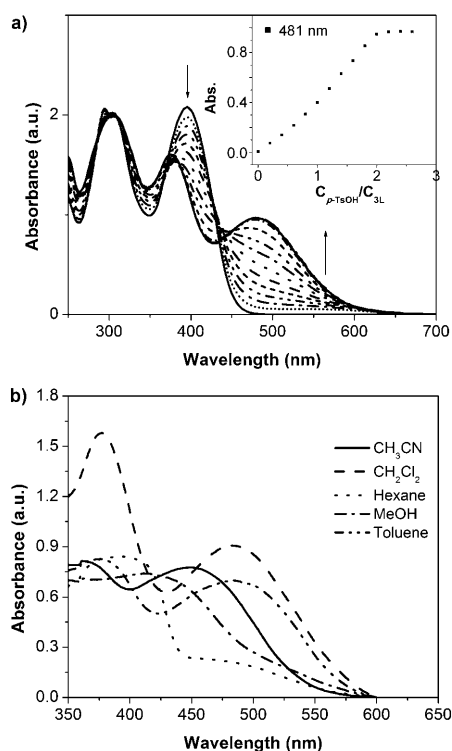


Figure 2. a) UV/Vis spectra of **3L** in CH_2Cl_2 with addition of *p*-TsOH/ CH_3CN solution. b) UV/Vis spectra of **3L** in different solvents with addition of 3 equiv of *p*-TsOH ($c = 4.9 \times 10^{-5} \text{ mol L}^{-1}$).

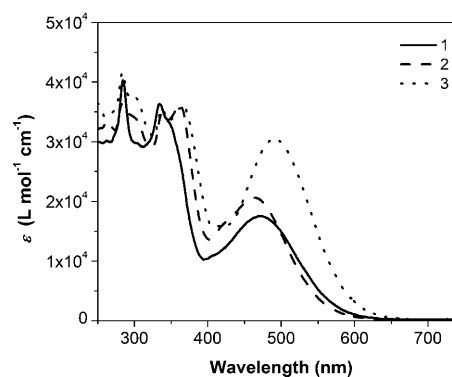


Figure 3. UV/Vis absorption spectra of **1**, **2**, and **3** in CH_3CN at a concentration of $1 \times 10^{-5} \text{ mol L}^{-1}$.

intense absorption bands below 370 nm, which are assigned as the ${}^1\pi,\pi^*$ transitions from the ligand. In addition, all complexes exhibit a broad intense absorption band in the visible region between 400 and 650 nm. The energies of these absorption bands are similar to those observed from the protonated ligands, implying that these bands possess an intraligand charge transfer (${}^1\text{ILCT}$) character from the diphenylamino component to the terpyridine component. Moreover, with respect to the other platinum terpyridyl chloride complexes,^[19] this band possibly possesses some metal-to-ligand charge transfer character (${}^1\text{MLCT}$). In addition, considering the large extinction coefficient of this absorption band, we speculate that this band could have some ${}^1\pi,\pi^*$ character. The charge-transfer nature of the low-energy absorption band is supported by the pronounced negative solvatochromic effect, as shown in Supporting Information Figure S2 for complex **2** and listed in Supporting Information Table S1 for complex **1**, which is similar to that observed from the low-energy charge transfer absorption band in the protonat-

ed ligands. For example, the low-energy absorption band maximum for **1** is 522 nm in hexane, which is 48 nm red-shifted compared to that in CH₃CN. Therefore the low-energy absorption band for **1–3** is tentatively assigned as a mixture of ¹ILCT/¹π,π*/¹MLCT. The mixed configurationally distinct transitions in the low-energy absorption band could be further supported by the energy trend of this band, which follows **2** > **1** > **3** and is inconsistent with that observed for the respective ligand. This could reflect a different degree of involvement of the charge transfer character in **2** compared to that in **1** and **3**. Unfortunately, this speculation could not be confirmed without the DFT calculation, which is not available at this time.

Photoluminescence: All ligands and platinum complexes are emissive at room temperature in solutions and at 77 K in glassy matrix. The room temperature emission spectra of **1L**, **2L**, and **3L** in CH₂Cl₂ are shown in Figure 4, and the emission data are summarized in Table 1. The emission of **1L**, **2L** and **3L** occurs at 484, 505, and 526 nm in CH₂Cl₂, respectively, with a high emission quantum yield (Φ_{em}) of 0.59, 0.70 and 0.42 for **1L**, **2L**, and **3L**, respectively. The emission energy decreases from **1L** to **3L**, which is in line with the trend observed for the UV/Vis absorption. The emission of the ligands is highly sensitive to the polarity of solvent. As exemplified in Supporting Information Figure S3 for **1L** in different solvents, a drastic positive solvatochromic effect is observed, for example, the emission in CH₃CN (510 nm) is much red-shifted compared to that in hexane (406 nm), which is indicative of a charge-transfer emitting state. The positive solvatochromic effect suggests that the emitting excited state is more polar than the ground state, which should be the ¹ICT state. Similar phenomena were observed for **2L** and **3L**. However, the excitation spectra monitored at the emission band maxima resemble those of the ¹π,π*/¹ICT transitions in the UV/Vis absorption spectra (as exemplified in Supporting Information Figure S4 for **1L**), which implies that the emitting state could have ¹π,π* character as well. Therefore, the emission from the ligands can be regarded as a mixture of ¹ICT/¹π,π* characters. This is in line with the

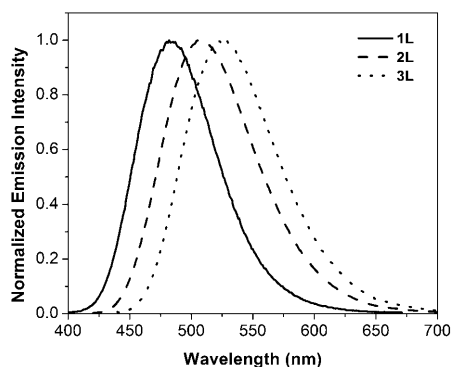


Figure 4. Normalized emission spectra of **1L** (λ_{ex} = 395 nm), **2L** (λ_{ex} = 390 nm), and **3L** (λ_{ex} = 395 nm) in CH₂Cl₂ ($c = 1 \times 10^{-5}$ mol L⁻¹).

dual fluorescence observed in many 4-aminobenzonitrile compounds.^[20]

The assignment of the emitting state of the ligands to mixed ¹ICT/¹π,π* states can be partially supported by the emission lifetime measurement using the 355 nm laser beam as excitation source. The emission from all ligands exhibits bi-exponential decays by deconvolution of the decay curve, with a short lifetime of tens of ns being attributed to the ¹ICT emission and a longer lifetime of approximately 100 ns being assigned to the ¹π,π* emission. In addition, the emission lifetime and intensity remain the same in argon-saturated solution compared to those in air-saturated solution. These results clearly indicate that the observed emission from the ligands is fluorescence from singlet excited state that admixes ¹π,π* and ¹ICT characters.

The emission spectra of platinum complexes **1–3** at room temperature upon excitation at wavelengths shorter than 400 nm are shown in Figure 5a. The emission energies for

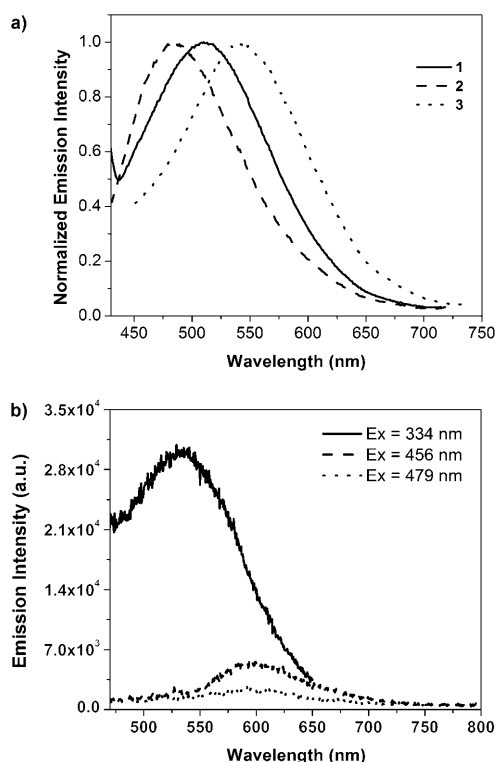


Figure 5. a) Normalized emission spectra of **1** (λ_{ex} = 384 nm), **2** (λ_{ex} = 374 nm), and **3** (λ_{ex} = 389 nm) in CH₃CN at room temperature ($c = 1 \times 10^{-5}$ mol L⁻¹). b) Emission spectra of **2** at different excitation wavelengths ($c = 5 \times 10^{-5}$ mol L⁻¹).

1–3 resemble those of their corresponding ligand. However, in contrast to the emission from the ligand, the emission energy of the complex decreases with increased concentration. As shown in Figure 6 for **2**, in the concentration range of 1×10^{-6} and 1×10^{-5} mol L⁻¹, the emission intensity increases with increased concentration and the emission

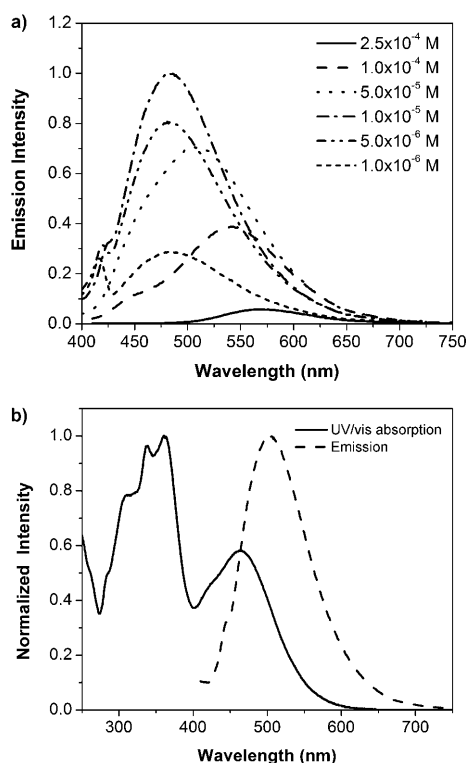


Figure 6. a) Concentration-dependent emission spectra of **2** in CH_3CN solutions at room temperature. b) Normalized UV/Vis and emission spectra of **2** in CH_3CN ($c = 1 \times 10^{-5} \text{ mol L}^{-1}$).

energy remains essentially the same. At higher concentration solutions ($5 \times 10^{-5} - 2.5 \times 10^{-4} \text{ mol L}^{-1}$), the emission intensity decreases and the emission band maximum bathochromically shifts. In view of the significant overlap of the low-energy absorption band in the UV/Vis absorption spectrum and the high-energy end of the emission band (shown in Figure 6b), the decreased emission intensity and emission energy should be attributed to re-absorption of the emission. A similar effect is observed for **1** and **3**. Other differences between the emission from the ligands and the complexes include the drastically reduced emission quantum yield and the much shorter lifetime of **1**, **2**, and **3** compared to those of their corresponding ligand. On the other hand, consistent with the emission from the ligands, the emission from the complexes is also independent of oxygen. The much shorter lifetime and the oxygen-independence suggest that the emission of the complexes upon excitation below 400 nm emanates from a singlet excited state. In view of the similarity of the emission energies of the platinum complexes to those of their corresponding ligand, and of the excitation spectra of the complexes to those of the ${}^1\pi,\pi^*/{}^1\text{ICT}$ transitions in the UV/Vis absorption of the corresponding ligand, and the similar positive solvatochromic effect (Figure S5), we tentatively assign the observed emission upon excitation below 400 nm to ${}^1\pi,\pi^*/{}^1\text{ILCT}$ states.

Upon excitation at the low-energy ${}^1\text{ILCT}/{}^1\pi,\pi^*/{}^1\text{MLCT}$ band, a very weak, structureless emission appears at approx-

imately 570 nm for **1**, 590 nm for **2**, and 620 nm for **3**, as exemplified in Figure 5b for **2**. This band becomes the dominant emission band in low-polarity solvents, such as in toluene and hexane, and a drastic negative solvatochromic effect is observed (see Supporting Information Figure S6 and Table S1 for complex **1**). The excitation spectra monitored at this low-energy emission band resemble the low-energy ${}^1\text{ILCT}/{}^1\pi,\pi^*/{}^1\text{MLCT}$ band in their UV/Vis spectra. These facts suggest that the low-energy emission band should originate from the charge transfer state(s), which is consistent with that reported for the 4-aminobenzonitrile compounds.^[20] In view of this emission band falling into the broad envelop of the spectrum obtained at excitation below 400 nm that shows biexponential decay, we can conclude that the emission spectra of **1–3** (Figure 5a) obtained upon excitation below 400 nm indeed compose ${}^1\pi,\pi^*/{}^1\text{ILCT}$ characters. However, the involvement of the ${}^1\text{MLCT}$ character cannot be excluded in view of the energy trend ($2 > 1 > 3$) observed for these complexes, which is consistent with that observed for the low-energy ${}^1\text{ILCT}/{}^1\pi,\pi^*/{}^1\text{MLCT}$ absorption band. This phenomenon suggests the involvement of the ${}^1\text{MLCT}$ character in the emitting state but the degree of ${}^1\text{MLCT}$ involvement is different in **2** compared to that in **1** and **3**.

To verify the involvement of ${}^1\text{ICT}$ or ${}^1\text{ILCT}$ character into the emitting states of the ligands and the platinum complexes, the emission of the protonated ligands has been investigated. Figure 7 shows the emission spectra of **3L** with

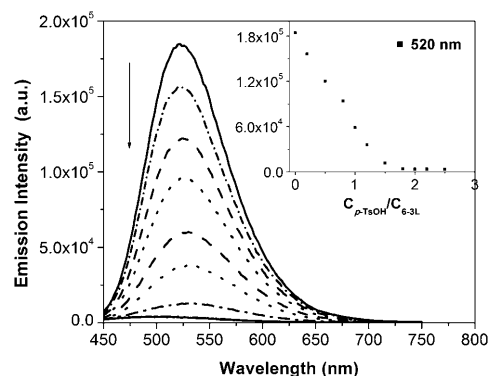


Figure 7. Room temperature emission spectra of **3L** ($c = 5.3 \times 10^{-5} \text{ M}$) in CH_2Cl_2 with addition of $p\text{-TsOH}/\text{CH}_3\text{CN}$ solution. $\lambda_{\text{ex}} = 396 \text{ nm}$.

addition of $p\text{-TsOH}$. Upon addition of $p\text{-TsOH}$, the emission of **3L** at about 502 nm decreases. This can be rationalized by the fact that protonation of the nitrogen atoms on the terpyridine increases the electron-withdrawing ability of the terpyridine component, which in turn results in enhanced ${}^1\text{ICT}$ or ${}^1\text{ILCT}$ character and quenches the emission. This result is in line with the increased ${}^1\text{ICT}$ or ${}^1\text{ILCT}$ character observed in the UV/Vis absorption spectra of the ligands and the complexes, and also partially accounts for the very low emission quantum yields of the platinum complexes upon excitation at 436 nm (Table 1).

As discussed earlier, the emission of **1–3** is assigned as the mixture of $^1\pi,\pi^*/^1\text{ILCT}$ characters, similar to those of their corresponding ligands, although the emission of **1–3** also possibly admixes some $^1\text{MLCT}$ character. However, the emission quantum yields and the emission lifetimes are much lower or shorter than those of the respective ligand. These differences could be rationalized by the following three possible reasons. First, the coordination of platinum(II) ion with the terpyridine ligand decreases the electron density on the terpyridine ligand, which increases the electron-withdrawing ability of the terpyridine component and enhances the charge transfer character of the complexes. Consequently, the emission from the complexes is quenched, which has been demonstrated by the ligand titration experiment. Secondly, the heavy-metal effect of the platinum increases the intersystem crossing from the singlet excited state to the triplet excited state. However, the triplet excited state is weakly-emissive due to the low-lying excited state that facilitates the decays through nonradiative relaxation to ground state; alternatively, it may decay through thermally accessible low-lying non-emissive $^3\text{d},\text{d}$ state. Thirdly, the decreased emission quantum yield may be also caused by the re-absorption due to the partial overlap of the low-energy absorption band and the emission spectrum.

The assignment of the emission of **1**, **2** and **3** at room temperature as fluorescence is further supported by the emission measurement at 77 K, which generally measures the emission from the triplet excited state. As shown in Figure 8

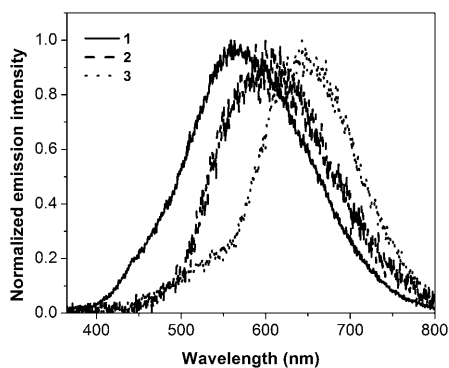


Figure 8. Emission spectra of **1–3** at 77 K in butyronitrile ($c = 1 \times 10^{-5} \text{ mol L}^{-1}$, $\lambda_{\text{ex}} = 355 \text{ nm}$).

for **1**, **2**, and **3** in butyronitrile at 77 K upon excitation at 355 nm, all complexes exhibit weak and broad emission at 77 K, which is obviously red-shifted compared to the emission at room temperature upon excitation below 400 nm. The lifetimes deduced from the decay of emission are of the order of tens to hundreds of μs , indicating that the emission of all complexes at 77 K originates from the $^3\pi,\pi^*$ state. The emission from the ligands **1L**, **2L**, and **3L** with 10 equivalents of CH_3I in 4:1 EtOH/MeOH was also observed (CH_3I was added as the external heavy atom to promote the inter-

system crossing from the singlet to the triplet excited states in order to observe the phosphorescence) and the results are summarized in Table 1. The emission lies in the similar energy levels as those of the complexes. Therefore, the emission for **1L**, **2L**, and **3L** at 77 K is also attributed to the phosphorescence from the $^3\pi,\pi^*$ state. However, the lifetime of the emission of **1L**, **2L**, and **3L** at 77 K cannot be measured due to the very weak emission.

Nanosecond transient absorption: The triplet excited-state absorption of **1L**, **2L**, and **3L** were studied by excitation with 4.1 ns 355 nm laser pulse. The time-resolved spectra are exemplified in Figure 9 for **1L**. The spectra for **2L** and **3L**

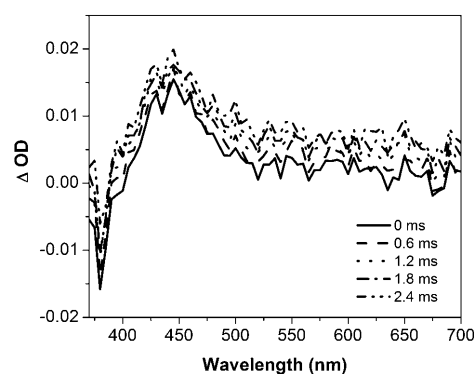


Figure 9. Time-resolved triplet transient difference absorption spectra of **1L** in CH_2Cl_2 . $\lambda_{\text{ex}} = 355 \text{ nm}$. The concentration of the solution was adjusted to obtain $A = 0.4$ at 355 nm in a 1 cm cuvette.

are provided in the Supporting Information Figure S7. A positive absorption band was observed at 445, 480, and 515 nm for **1L**, **2L** and **3L**, respectively. The lifetime of the transient species are too long to be measured on our instrument (in the ms region). The energy of the transient absorption band maximum decreases from **1L** to **3L**, which is consistent with the trends observed from the UV/Vis absorption and the emission measurements. Because of the ultralong lifetime of the transient species, we propose that the transient absorption arises from the $^3\pi,\pi^*$ of the ligand, especially from the $^3\pi,\pi^*$ state of the fluorene component, which was reported to occur around 406 nm extending to 600 nm in the literature.^[21] In contrast, no triplet excited-state absorption was observed for **1–3** at room temperature, possibly due to the short-lived triplet excited state.

Femtosecond transient absorption: As discussed earlier, **1–3** exhibit fluorescence at room temperature and the transient absorption from the triplet excited state was not detected. To further investigate the singlet excited-state properties of **1**, **2**, and **3**, the measurements of singlet excited-state absorption of these complexes were carried out using ultrafast femtosecond laser excitation (260 fs) at 400 nm. The transient difference absorption spectra at different decay time along with the ground-state absorption spectrum are exemplified in Figure 10 for **1**. All complexes possess a bleaching

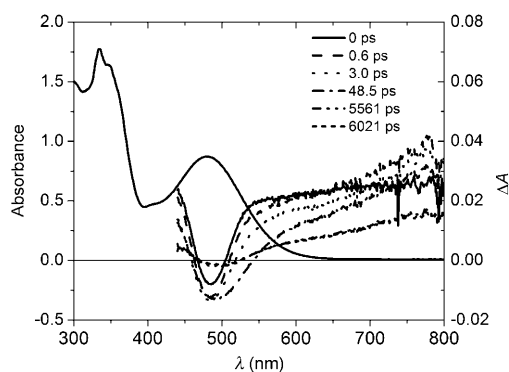


Figure 10. Time-resolved femtosecond transient difference absorption spectra and ground-state absorption spectrum of **1** in CH_3CN . $\lambda_{\text{ex}} = 400$ nm.

Table 2. Femtosecond transient absorption data of **1–3** in CH_3CN .

	1	2	3
$\lambda_{\text{S}_1-\text{S}_0}$ [nm]	554, 780	549	590
τ_1 [ps]	0.5 ± 0.5	fast	fast
τ_2 [ps]	3.9 ± 1.7	2.4 ± 0.5	3.4 ± 1.2
τ_3 [ps]	62 ± 46	136 ± 128	272 ± 95
τ_4 [ps]	4070 ± 2262	2858 ± 1001	3945 ± 2480

band in the region where the ${}^1\pi,\pi^*/{}^1\text{ILCT}/{}^1\text{MLCT}$ absorption band appears, and a broad, moderately strong positive absorption band from 510 nm extending to the near-IR region. The lifetimes obtained from the fitting of the decay curves are summarized in Table 2. The decay of the transient species consists of four components: a very fast decay (τ_1) due to the intramolecular vibrational relaxation (IVR) from the upper excited vibrational levels; a decay in the region of 2–4 ps (τ_2) associated with solvent reorganization around the excited molecule; a decay of tens to hundreds of ps (τ_3) and a longer decay of several ns (τ_4). The magnitude of τ_3 and τ_4 coincides with the lifetime deduced from the decay of the room temperature emission from these complexes. Therefore, the excited state that gives rise to the observed transient absorption can be considered as the same excited state that emits, that is, ${}^1\pi,\pi^*/{}^1\text{ILCT}$, maybe mixed with some ${}^1\text{MLCT}$ character, which is supported by the consistence of the bleaching band with the ${}^1\pi,\pi^*/{}^1\text{ILCT}/{}^1\text{MLCT}$ absorption band.

Two-photon absorption: Because of the conjugated structure and the charge-transfer nature of the ligands and the complexes, it is expected that all ligands and complexes exhibit at least a moderately strong two-photon absorption (2PA) ($\sigma_2 > 100$ GM, $1 \text{ GM} = 10^{-50} \text{ cm}^4 \text{ s photon}^{-1} \text{ molecule}^{-1}$) upon NIR excitation. The 2PA spectra of **1L**, **2L**, and **3L** in toluene were measured by two-photon excited fluorescence method^[22] and the results are shown in Figure 11. The 2PA band maxima of **1L–3L** almost coincide with their corresponding 1PA band maxima. Because of the lack of center of symmetry of these ligands and the approximate overlap with the 1PA peak, we conclude that the lowest-energy 2PA

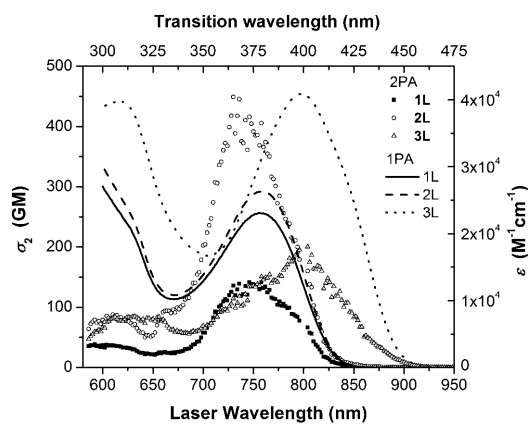


Figure 11. Two-photon absorption spectra (symbols) and one-photon absorption spectra (solid lines) of **1L–3L** in toluene. The experimental error for the TPA spectra measurement is approximately $\pm 30\%$.

transitions of the ligands correspond to the $\text{S}_0 \rightarrow \text{S}_1$ transitions. Compounds **1L**, **2L**, and **3L** exhibit the maximum σ_2 value of 142, 448, and 204 GM, respectively, at 750 nm. The general trend of the σ_2 value follows the sequence: $\sigma_2(\mathbf{2L}) > \sigma_2(\mathbf{3L}) > \sigma_2(\mathbf{1L})$. The stronger 2PA in **2L** than in **3L** should be attributed to the better conjugation provided by the ethynylene bridge, which avoids the twisting of the fluorenyl component out of the conjugation in comparison to a vinylene linker. The similar effect has been reported for ethynylene-linked porphyrin and the vinylene-linked porphyrin.^[23]

Even though the peak σ_2 values for the ligands are not particularly large, they are comparable to the values in similar structures such as BDPAS (4,4'-bis(diphenylamino)stilbene), in which $\sigma_2 = 230$ GM at 650 nm.^[22] It is expected that increasing the dipole moment difference between S_0 and S_1 , for example, by strengthening the intraligand charge transfer in the ligand, will augment the 2PA cross-section. After coordination with the platinum ion, the intraligand charge transfer is enhanced, which is reflected by the red-shift of the low-energy absorption band in the UV/Vis absorption spectra of the complexes. Thus, it is anticipated that the platinum complexes exhibit stronger 2PA at the near-IR region. Unfortunately, due to the very low quantum yield ($\Phi_f < 0.05\%$) and further attenuation of the fluorescence by the low-energy absorption band, we were unable to measure the 2PA spectrum and cross-sections of the complexes via the 2PA excited fluorescence method. To overcome this obstacle, we carried out wavelength dependent open-aperture Z-scan^[24] measurements using 21 ps duration NIR pulses. To properly account for possible stepwise absorption from the excited states, we fitted the experimental data using a five-band model,^[25] which includes both the excited-state absorption and the two-photon absorption. In order to disambiguate the relative contributions of two-photon and excited-state absorption at those wavelengths at which the two-photon process represents the dominant mechanism for populating the excited states, the singlet excited-state absorption cross-section $\sigma_s(\lambda)$ was estimated from the fs transient absorption spectrum at zero time delay and only $\sigma_2(\lambda)$

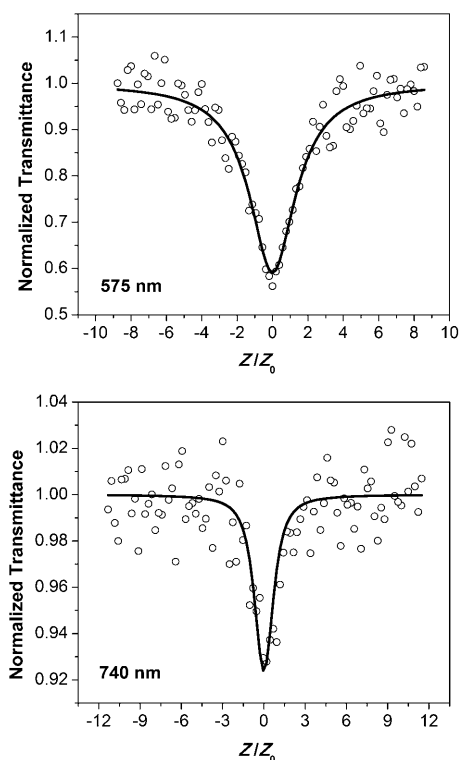


Figure 12. Open-aperture Z-scan experimental data and fitting curves for **2** in CH_3CN at different wavelengths. The energy used for the experiment was 2.7 μJ at 575 nm and 6.6 μJ at 740 nm, and the beam waist at the focal point was 31 μm .

was used as a fitting parameter. Nonlinear absorption was observed from 575 nm to 740 nm for **1**, 550 nm to 825 nm for **2**, and 575 nm to 670 nm for **3**. Figure 12 shows the typical nonlinear absorption data and the fitting curves at two different wavelengths for **2**. For all three complexes, there is measurable ground-state absorption at the wavelengths shorter than 670 nm. The nonlinear absorption observed at these wavelengths relates most likely to the transient absorption from the excited S_1 state. Calculations of the excited-state population during one laser pulse excitation indicate that at wavelengths shorter than 670 nm, all three complexes also have significant S_2 populations (reaching a maximum of ~20–40%, see Supporting Information Figure S8 for complex **2** at 575 nm). However, except for the 575 nm Z scan of **3** (which represents something of a special case), one cannot unambiguously separate the effects of excited-state absorption from S_1 from the effects of excited-state absorption from S_2 using the data available at this time. For this reason, the $\sigma_S(\lambda)$ values quoted in Table 3 should be interpreted as effective values representing a weighted average of the effects of excited-state absorption from S_1 and S_2 , in which the former contribution is dominant; they were obtained by setting $\sigma_S(\lambda)$ equal to $\sigma_{S_2}(\lambda)$ and fitting with a single free parameter. At wavelengths longer than 740 nm, the nonlinear absorption is attributed to the two-photon induced excited-state absorption. As previously noted, at each of these wavelengths the singlet excited-state absorption

Table 3. Excited-state absorption and two-photon absorption cross-sections for **1–3** at different wavelengths.

Complex	λ [nm]	σ_0 [10^{-18} cm^2] ^[a]	σ_S [10^{-18} cm^2] ^[b]	σ_S/σ_0	σ_2 [GM]
1	575	10.1	20 ± 1	2.0	
	600	3.83	20 ± 2	5.2	
	630	0.956	17 ± 1	18	
	670	0.191	25 ± 1	131	
	740		24.4 ^[c]		850 ± 50
2	550	14.7	38 ± 2	2.6	
	575	6.31	24 ± 2	3.8	
	600	2.49	24 ± 2	9.6	
	630	0.765	26 ± 2	34	
	680	0.153	12 ± 1	78	
	740		7.7 ^[c]		1200 ± 100
	760		11.1 ^[c]		1000 ± 200
	800		7.7 ^[c]		2000 ± 200
825		11.6 ^[c]		600 ± 100	
3	575	25.8	43 ± 5 ^[d]	1.7	
	600	10.9	36 ± 2	3.3	
	630	3.63	20 ± 2	5.5	
	670	0.765	16 ± 1	21	

[a] Ground-state absorption cross-section. [b] Effective singlet excited-state absorption cross-section with the assumption of $\sigma_{S_2} = \sigma_S$. [c] Estimated from the fs TA data at zero time delay. [d] $\sigma_{S_2} = (12 \pm 7) \times 10^{-18}$ cm^2 .

cross-section deduced from the fs transient absorption measurement at zero-time delay was treated as a fixed parameter, and the Z-scan data were fit using the 2PA cross-section as the sole fitting parameter. As shown in Table 3, the σ_2 obtained for **1** and **2** are all much larger than those of their respective ligands. To the best of our knowledge, these σ_2 values are also the largest values reported for platinum complexes to date. It is noted that **2** exhibits a broader 2PA than **1**, and the σ_2 value is larger for **2** than that for **1** at the corresponding wavelength. This is consistent with the trend observed from the corresponding ligands. For complex **3**, the 2PA was too weak to be observed. The stronger 2PA in **2** than in **3** should also be attributed to the better conjugation provided by the ethynylene bridge, similar to that discussed earlier for the ligands. However, it is worthy of noting that the σ_2 values obtained by the Z-scan method could be overestimated compared to those obtained by the two-photon excited fluorescence method. Nevertheless, the trend of σ_2 values observed for these complexes should still be valid.

Conclusion

Three dipolar D- π -A terpyridine ligands and their platinum complexes have been successfully synthesized and characterized. All dipolar terpyridine ligands are highly emissive at room temperature. The emitting excited state is assigned as the admixture of $^1\pi,\pi^*$ and ^1ICT characters for the ligands. The corresponding platinum complexes exhibit weak fluorescence from the singlet excited state of $^1\pi,\pi^*/^1\text{ILCT}$ at room temperature, possibly mixed with some $^1\text{MLCT}$ character. The assignment of the emitting state to $^1\pi,\pi^*/^1\text{ILCT}/^1\text{MLCT}$ excited state when excited below 400 nm is consistent with the femtosecond transient differ-

ence absorption measurement. The dipolar terpyridine ligands **1L**, **2L**, and **3L** exhibit two-photon absorption at the near-IR region, with the 2PA band maxima coincide with their respective 1PA band maxima. The general trend of the 2PA cross-section (σ_2) value follows the sequence of $\sigma_2(\mathbf{2L}) > \sigma_2(\mathbf{3L}) > \sigma_2(\mathbf{1L})$, suggesting that triple bond connection between the donor and acceptor favors the 2PA. The maximum 2PA cross-section was obtained to be 448 GM in **2L**. The σ_2 values of the platinum complexes (600–2000 GM) measured by Z-scan experiment are much larger than those of their corresponding ligands, with the largest σ_2 value to be 2000 GM at 800 nm for **2**. To the best of our knowledge, these values are the largest σ_2 values reported for platinum complexes to date. Complex **2** with the ethynylene linker shows much stronger 2PA than complex **3** with the vinylene linker. However, we should point out that the σ_2 values obtained by the Z-scan method could be overestimated compared to those obtained by the two-photon excited fluorescence method.

Experimental Section

Synthesis: All reagents and solvents (analytical grade) were purchased from VWR Scientific Company and used without further purification unless otherwise stated. The silica gel (230–400 mesh) was purchased from Alfa Aesar Company. Neutral Al_2O_3 (standard grade, 150 mesh) was purchased from Aldrich Company. All products were characterized by ^1H NMR, elemental analysis, and HRMS. ^1H NMR spectra were obtained using a Varian 400 MHz or 500 MHz VNMR spectrometer. HRMS was conducted on a Bruker Daltonics BioTOF system with electrospray ionization (ESI) source. Elemental analyses were conducted by NuMega Resonance Labs, Inc. in San Diego, CA.

The precursors 2-iodofluorene (**5**),^[26] 2-bromo-7-iodofluorene (**6**),^[18] 2-bromo-9,9-di(2-ethylhexyl)-7-iodofluorene (**7**), 2-bromo-9,9-di(2-ethylhexyl)-7-diphenylaminofluorene (**8**),^[18] 4'-bromo-2,2':6',2''-terpyridine,^[27] 4'-vinyl-2,2':6',2''-terpyridine (**12**),^[28] 4'-(trifluoromethyl)sulfonyloxy-2,2':6',2''-terpyridine (OTf-tpy),^[28] were synthesized according to the procedures reported in the literature.

2-Bromo-9,9-di(2-ethylhexyl)-7-diphenylaminofluorene (8): 2-Bromo-9,9-di(2-ethylhexyl)-7-iodofluorene (**7**) (7.00 g, 0.012 mol), diphenylamine (2.58 g, 0.015 mol), [18]crown-6 (0.26 g, 0.001 mol), Cu (1.50 g, 0.023 mol), and K_2CO_3 (2.60 g, 0.019 mol) were added to mesitylene (40 mL). The mixture was heated to reflux under argon overnight. After the solvent was removed, the residue was dissolved in Et_2O . The organic phase was washed with water, and dried over MgSO_4 . After removal of the solvent, the crude product was purified by a silica gel column using hexane to give a colorless oil (4.50 g, 42%). ^1H NMR (400 MHz, CDCl_3): δ = 0.56 (m, 8H), 0.75–1.00 (m, 22H), 1.73–1.92 (m, 4H), 7.00–7.12 (m, 8H), 7.25 (m, 4H), 7.46 (m, 3H), 7.55 ppm (m, 1H).

7-(4,4,5,5-Tetramethyl-1,3,2-dioxaborolan-2-yl)-9,9-di(2-ethylhexyl)fluoren-2-yl-diphenylamine (9): Compound **8** (1.0 g, 1.12 mmol) was dissolved in dried THF (50 mL) at -78°C . 1.6 M BuLi/hexane solution (2.0 mL, 3.20 mmol) was added slowly. The mixture was stirred at -78°C for 1 h. 2-Isopropoxy-4,4,5,5-tetramethyl-1,3,2-dioxaborolane (0.42 mL, 1.12 mmol) was added dropwise. The mixture was allowed to reach room temperature and stirred at RT overnight. After that brine (50 mL) was added to terminate the reaction. The aqueous layer was extracted with Et_2O (3×30 mL). The combined organic layer was dried over Na_2SO_4 . After removal of the solvent, the crude product was purified by a silica gel column using hexane/toluene 5:1 to give a colorless oil (735 mg, 70%). ^1H NMR (400 MHz, CDCl_3): δ = 0.50 (m, 8H), 0.6–0.9 (m, 22H),

1.34 (s, 12H), 1.7–2.0 (m, 4H), 6.9–7.1 (m, 8H), 7.21 (m, 4H), 7.58 (m, 2H), 7.76 ppm (m, 2H).

Ligand 1L: Compound **9** (0.75 g, 0.80 mmol) and 4'-bromo-2,2':6',2''-terpyridine (311 mg, 1.00 mmol) were added to toluene (50 mL). 2 M K_2CO_3 aqueous solution (2.5 mL) was added. The mixture was degassed in argon for 20 min. $[\text{Pd}(\text{PPh}_3)_4]$ (46 mg, 0.04 mmol) was added. The mixture was heated to reflux under argon overnight. The organic layer was washed with water, dried over MgSO_4 and filtered. After the solvent was removed, the crude product was purified on a silica gel column eluted by CH_2Cl_2 to give a pale yellow solid (422 mg, 67%). ^1H NMR (500 MHz, CDCl_3): δ = 0.6 (m, 8H), 0.7–1.0 (m, 22H), 1.86–2.10 (m, 4H), 7.03 (m, 2H), 7.11 (m, 6H), 7.16 (m, 4H), 7.38 (t, $J=6.5$ Hz, 2H), 7.66 (m, 1H), 7.76 (m, 1H), 7.86 (t, $J=7.0$ Hz, 2H), 7.91 (2H, t, $J=7.0$ Hz), 8.70 (d, $J=8.0$ Hz, 2H), 8.78 ppm (m, 4H); HRMS: m/z (%): calcd for $[\text{C}_{56}\text{H}_{61}\text{N}_4]^+$: 789.4891; found: 789.4875 (100).

Complex 1: Ligand **1L** (560 mg, 0.71 mmol) and $[\text{Pt}(\text{dmsO})_2\text{Cl}_2]$ (300 mg, 0.73 mmol) were added to CHCl_3 (80 mL). The mixture was heated to reflux under argon for 24 h. After the solvent was removed, the residue was purified on an Al_2O_3 column eluted by CH_2Cl_2 , followed by $\text{CH}_2\text{Cl}_2/\text{MeOH}$ 1:1. The crude product was purified by recrystallization from $\text{CH}_2\text{Cl}_2/\text{hexane}/\text{Et}_2\text{O}$ to give a red solid (486 mg, 65%). ^1H NMR (500 MHz, CDCl_3): δ = 0.6 (m, 8H), 0.7–1.2 (m, 22H), 2.0 (m, 2H), 2.35 (m, 2H), 7.13 (m, 8H), 7.29 (m, 4H), 7.48 (m, 2H), 7.70 (d, $J=8.0$ Hz, 1H), 7.97 (d, $J=8.0$ Hz, 1H), 8.32 (m, 3H), 8.53 (m, 3H), 8.77 (t, $J=8.0$ Hz, 2H), 9.11 ppm (d, $J=7.5$ Hz, 2H); HRMS: m/z (%): calcd for $[\text{C}_{56}\text{H}_{60}\text{N}_4\text{PtCl}]^+$: 1019.4156; found: 1019.4159 (100); elemental analysis calcd (%) for $\text{C}_{56}\text{H}_{60}\text{N}_4\text{PtCl}_2 \cdot 2.5 \text{CH}_2\text{Cl}_2$: C 55.30, H 5.12, N 4.41; found: C 55.75, H 5.30, N 4.57.

Compound 10: Compound **8** (1.10 g, 1.70 mmol) and 2-methyl-3-butyn-2-ol (0.33 mL, 3.40 mmol) was added to triethylamine (30 mL). CuI (7.00 mg, 0.04 mmol), PPh_3 (18.00 mg, 0.07 mmol), and $[\text{Pd}(\text{PPh}_3)_4]$ (50.0 mg, 0.04 mmol) were added. The mixture was heated to reflux under argon overnight. The solvent was removed, and the residue was dissolved in CH_2Cl_2 . The solution was washed with water, and dried over Na_2SO_4 . After the solvent was removed, the crude product was purified on a silica gel column eluted by hexane/ CH_2Cl_2 1:1 to give a colorless oil (435 mg, 40%). ^1H NMR (400 MHz, CDCl_3): δ = 0.46–0.53 (m, 8H), 0.68–0.86 (m, 22H), 1.62 (t, $J=2.8$ Hz, 6H), 1.75–1.89 (m, 4H), 1.99 (t, $J=3.2$ Hz, 1H), 7.01 (m, 8H), 7.22 (m, 4H), 7.34 (m, 2H), 7.52 ppm (m, 2H).

Compound 11: Compound **10** (0.41 g, 0.64 mmol) and KOH (0.30 g, 5.36 mmol) were added to 2-propanol (10 mL). The mixture was heated to reflux under argon for 3 h. After the solvent was removed, the residue was purified on a silica gel column eluted by hexane to give a colorless oil (268 mg, 72%). ^1H NMR (400 MHz, CDCl_3): δ = 0.51 (m, 8H), 0.68–0.90 (m, 22H), 1.55–1.99 (m, 4H), 3.06 (s, 1H), 6.96–7.06 (m, 8H), 7.23 (m, 4H), 7.42 (m, 2H), 7.53 ppm (m, 2H); HRMS: m/z (%): calcd for $[\text{C}_{43}\text{H}_{51}\text{N}]^+$: 581.4016; found: 581.4019 (100).

Ligand 2L: Compound **11** (323 mg, 0.56 mmol) and OTf-tpy (212 mg, 0.56 mmol) were added to a mixture of benzene (50 mL) and isopropylamine (20 mL). $[\text{Pd}(\text{PPh}_3)_4]$ (30 mg, 0.02 mmol) was then added. The mixture was heated to reflux under argon overnight. After the solvent was removed, the residue was dissolved in CH_2Cl_2 . The solution was washed with water, and dried over Na_2SO_4 . After the solvent was removed, the crude product was purified on a neutral Al_2O_3 column eluted by hexane/ CH_2Cl_2 10:1 to remove the unreacted reagent, and then eluted with hexane/ CH_2Cl_2 1:1 to give a pale yellow solid (341 mg, 75%). ^1H NMR (400 MHz, CDCl_3): δ = 0.58 (m, 8H), 0.7–1.0 (m, 22H), 1.8–2.0 (m, 4H), 7.0 (m, 8H), 7.23 (t, $J=8.1$ Hz, 4H), 7.35 (m, 2H), 7.57 (m, 4H), 7.87 (dt, $J=7.5, 1.5$ Hz, 2H), 8.63 (m, 4H), 8.74 ppm (dt, $J=4.8$ Hz, 2H); HRMS: m/z (%): calcd for $[\text{C}_{58}\text{H}_{61}\text{N}_4]^+$: 813.4891; found: 813.4917 (100).

Complex 2: Ligand **2L** (340 mg, 0.42 mmol) and $[\text{Pt}(\text{dmsO})_2\text{Cl}_2]$ (212 mg, 0.52 mmol) were added to CHCl_3 (80 mL). The mixture was heated to reflux under argon for 24 h. After the solvent was removed, the residue was purified by an Al_2O_3 column eluted first by $\text{CH}_2\text{Cl}_2/\text{CH}_3\text{CN}$ 5:2, and then by $\text{CH}_2\text{Cl}_2/\text{MeOH}$ 10:1. The crude product was further purified by recrystallization from $\text{CH}_2\text{Cl}_2/\text{hexane}/\text{Et}_2\text{O}$ to give a red solid (258 mg, 57%). ^1H NMR (400 MHz, CDCl_3): δ = 0.6 (m, 8H), 0.7–1.0 (m, 22H),

1.8–2.0 (m, 4H), 7.10 (m, 8H), 7.26 (m, 4H), 7.52 (m, 1H), 7.60 (m, 2H), 7.70 (m, 2H), 8.20 (m, 2H), 8.40 (t, $J=8.0$ Hz, 2H), 8.87 (d, $J=8.0$ Hz, 2H), 9.01 (d, $J=4.8$ Hz, 2H), 9.29 ppm (s, 2H); HRMS: m/z (%): calcd for $[\text{C}_{38}\text{H}_{60}\text{N}_4\text{PtCl} + \text{C}_2\text{H}_6\text{O} + \text{H}]^+$: 1089.4576; found: 1089.4543 (100); elemental analysis calcd (%) for $\text{C}_{38}\text{H}_{60}\text{N}_4\text{PtCl}_2 \cdot 0.8\text{CH}_2\text{Cl}_2 \cdot \text{CH}_3\text{CH}_2\text{OH}$: C 61.22, H 6.04, N 4.97; found: C 61.21, H 5.71, N 4.70.

Ligand 3L: Compound **8** (580 mg, 0.90 mmol), **12** (233 mg, 0.90 mmol) and $\text{P}(o\text{-tolyl})_3$ (100 mg, 0.33 mmol) were added to triethylamine (30 mL). $\text{Pd}(\text{OAc})_2$ (10 mg, 0.04 mmol) was then added. The mixture was heated to reflux under argon overnight. The mixture was filtered out and washed with Et_2O . The filtrate was washed with water. The organic phase was dried over Na_2SO_4 . The crude product was purified by a neutral Al_2O_3 column eluted by CH_2Cl_2 to give an orange viscous oil (571 mg, 78%). ^1H NMR (500 MHz, CDCl_3): δ = 0.6 (m, 8H), 0.7–1.0 (m, 22H), 1.8–2.1 (m, 4H), 7.15 (m, 9H), 7.25 (m, 4H), 7.40 (dd, $J=6.5, 1.5$ Hz, 2H), 7.59 (m, 2H), 7.67 (d, $J=7.5$ Hz, 2H), 7.93 (d, $J=16$ Hz, 2H), 7.92 (t, $J=7.5$ Hz, 2H), 8.57 (s, 2H), 8.72 (d, $J=7.5$ Hz, 2H), 8.80 ppm (d, $J=5.0$ Hz, 2H); HRMS: m/z (%): calcd for $[\text{C}_{38}\text{H}_{63}\text{N}_4]^+$: 815.5047; found: 815.5015 (100); elemental analysis calcd (%) for $\text{C}_{38}\text{H}_{62}\text{N}_4 \cdot \text{toluene} \cdot 1.5\text{H}_2\text{O}$: C 83.56, H 7.88, N 6.00; found: C 83.11, H 7.84, N 6.02.

Complex 3: Compound **3L** (91.8 mg, 0.11 mmol) and $[\text{Pt}(\text{dmsO})_2\text{Cl}_2]$ (47.6 mg, 0.12 mmol) were added to CHCl_3 (80 mL). The mixture was heated to reflux under argon for 24 h. After the solvent was removed, the residue was purified by an Al_2O_3 column eluted by CH_2Cl_2 , and then by $\text{CH}_2\text{Cl}_2/\text{MeOH}$ 1:1. The crude product was purified by recrystallization from $\text{CH}_2\text{Cl}_2/\text{hexane}/\text{Et}_2\text{O}$ to give a red solid (55.8 mg, 47%). ^1H NMR (400 MHz, CDCl_3): δ = 0.6 (m, 8H), 0.7–1.0 (m, 22H), 1.8–2.2 (m, 4H), 7.10 (m, 8H), 7.26 (m, 4H), 7.49 (m, 2H), 7.61 (m, 2H), 7.85 (m, 2H), 8.20 (m, 2H), 8.50 (m, 5H), 8.92 ppm (m, 2H); HRMS: m/z (%): calcd for $[\text{C}_{38}\text{H}_{62}\text{N}_4\text{PtCl}]^+$: 1045.4313; found: 1045.4339 (100); elemental analysis calcd (%) for $\text{C}_{38}\text{H}_{62}\text{N}_4\text{PtCl}_2 \cdot 2.5\text{CH}_2\text{Cl}_2$: C 56.18, H 5.22, N 4.33; found: C 56.09, H 5.32, N 4.66.

Photophysical measurements: The electronic absorption spectra were recorded on a SHIMADZU 2501 PC UV/Vis spectrophotometer. The emission spectra at room temperature were recorded on a SPEX Fluorolog-3 fluorometer/phosphorometer. Complexes **1**, **2**, and **3** were dissolved in CH_3CN , and ligands **1L**, **2L**, and **3L** were dissolved in CH_2Cl_2 . The solutions were degassed via bubbling Ar gas for 30 min prior to each measurement. The emission lifetimes of ligand **1L**, **2L**, and **3L** were measured on an Edinburgh LP920 laser flash photolysis spectrometer. The excitation beam was the third-harmonic output (355 nm) of a Quantel Brilliant Q-switched Nd/YAG laser (FWHM pulse width was 4.1 ns and the repetition rate was set at 1 Hz). The sample solutions were degassed for 30 min. before each measurement. The emission lifetime of complexes **1**, **2**, and **3** were measured by time correlated single photon counting (TCSPC) technique ($\lambda_{\text{ex}}=375$ nm). The sample solutions were prepared to have an absorbance at 375 nm of approximately 0.1–0.2. The emission quantum yields of the ligands **1L**, **2L**, and **3L**, and the complexes **1**, **2**, and **3** were determined by the comparative method,^[29] in which 9,10-diphenylanthracene in ethanol ($\Phi_{\text{em}}=0.9$, excited at 350 nm)^[30] was used as the reference for the ligands, and a degassed aqueous solution of $[\text{Ru}(\text{bpy})_3\text{Cl}_2]$ ($\Phi_{\text{em}}=0.042$, excited at 436 nm)^[31] was used as the reference for the complexes. The nanosecond triplet transient difference absorption spectra were measured on the Edinburgh LP920 laser flash photolysis spectrometer. The excitation was provided by the third-harmonic output (355 nm) of the Quantel Brilliant Q-switched Nd/YAG laser. The solutions were degassed via bubbling Ar gas for 30 min before each measurement. The absorbance of the solution was adjusted to $A=0.4$ at 355 nm in a 1 cm quartz cuvette. The femtosecond transient difference absorption spectra were measured on a femtosecond pump-probe UV/Vis spectrometer (HELIOS) manufactured by Ultrafast Systems LLC. The sample was excited at 400 nm with a 260 fs Ti/sapphire laser pulse, and the absorption was probed from 440 to 800 nm with white light continuum.

Two-photon induced fluorescence spectroscopic measurement: The 2PA spectra of the ligands **1L–3L** in toluene (toluene was chosen as the solvent instead of CH_2Cl_2 because the toluene solutions of **1L–3L** were

much stable than the CH_2Cl_2 solutions upon laser irradiation) were measured by modified fluorescent method. The measurements were done by monitoring the wavelength-dependent two-photon-excited fluorescence, which allowed for direct measurement of 2PA in a broad variety of compounds with the fluorescence (or phosphorescence) quantum yield $\Phi > 0.005$. The relative spectrum was measured using coumarin 485 in methanol as a reference with a 2 nm interval for both the sample and the reference. Then the spectrum was normalized to a correct cross-section measured at a single wavelength relative to 9,10-dichloroanthracene in dichloromethane.^[22]

The 2PA experimental setup and the detailed description of the experimental method were reported previously.^[22] The laser system comprises Ti/sapphire femtosecond oscillator (Coherent Mira 900) pumped with a CW frequency-doubled Nd/YAG laser (Coherent Verdi). The oscillator is used to seed a 1 kHz repetition rate Ti/sapphire femtosecond regenerative amplifier (Coherent Legend-HE). The output pulses from the amplifier are down-converted with an optical parametric amplifier (OPA) (Quantronix TOPAS-C). The output of the OPA (signal and idler) can be continuously tuned from 1100 to 2200 nm. For two-photon excitation we used second harmonic of either idler (790–1100 nm) or signal (550–790 nm) beam. A Glan-prism polarizer was placed before the second harmonic generation (SHG) crystal to select either vertical (signal) or horizontal (idler) polarization. The residual fundamental beam (signal or idler) was cut with color filters, placed after the SHG crystal. For one-photon excitation, the second harmonic of the Ti/sapphire amplifier output (397 nm) was used. The polarization of the excitation laser beam was vertical for both 1PA and 2PA. In the case of second harmonic of signal, a $\lambda/2$ plate was used after the reference detector to rotate polarization by 90°.

The fluorescence was collected at 90° to the laser beam direction with a spherical mirror ($f=50$ cm, mirror diameter $d=10$ cm), which focused the horizontally-elongated image of fluorescence track with the magnification ratio $\sim 1:1$ on the entrance plane of the fluorescence grating spectrometer (Jobin Yvon Triax 550). The height of the vertical spectrometer slit was much larger than the height of the fluorescence image. The spectral dispersion on a 2D CCD detector (Jobin Yvon Spectrum One) occurred in the horizontal direction, while the signal in the vertical direction was integrated over the whole slit height. The slit width was much smaller than the horizontal dimension of the fluorescence image and was kept the same in both 1PA and 2PA signal measurements. While recording the fluorescence spectrum, special care was taken to eliminate any spurious signals, such as scattered laser light, fluorescence of impurities, etc. The fluorescence spectra of the sample excited via 1PA and 2PA always had the same shape. The fluorescence intensity was measured by integrating the CCD output over 0.5–5 seconds and over 40–60 nm spectral region around the emission peak wavelength. Each data point was obtained by averaging of 2–5 acquisitions.

The raw spectra were obtained by measuring 2PA-excited fluorescence normalized to a square of the excitation laser power in a range of interest of excitation wavelengths. The absolute spectra were obtained by calibrating the unknown efficiency of fluorescence registration and fluorescence quantum yield and by correcting the raw spectra for the wavelength-dependent spatial and temporal laser profile.

Z-scan measurement and fitting: The open-aperture Z-scan experimental setup is similar to the one reported previously by our group.^[25] An optical parametric generator (EKSPLA PG401) pumped by the third harmonic output of an EKSPLA PL2143A passively mode-locked, Q-switched Nd:YAG laser (pulse width=21 ps, repetition rate=10 Hz) was used as the light source. A 25 cm or 30 cm plano-convex lens was used to focus the beam to a beam waist of ~ 30 μm at the focal point, which gave rise to a Rayleigh length ($z_0 = \pi\omega_0^2/\lambda$, where ω_0 is the radius at the beam waist) of approximately 3.4–4.9 mm at the spectral range used for the Z-scan study. Therefore, the sample solution placed in a 2 mm cuvette could be considered as thin samples. A 50 cm plano-convex lens was placed at approximately 30 cm after the linear focal plane to collect all of the transmitted light into the Molectron J4-09 joulemeter probe.

The experimental Z-scan data were fitted using the five-band model, in which each chromophore molecule is assumed to lie in the vibration-rotat-

tion manifold of one of five electronic states: the ground state, S_0 , a singlet; one of two singlet excited states, S_1 or S_2 ; or one of two triplet states, T_1 or T_2 . The following rate equations specify the time evolution of n_0 , n_S , n_T , n_{S2} , and n_{T2} , the number densities of molecules in, respectively, the S_0 , S_1 , T_1 , S_2 , and T_2 bands.

$$\frac{\partial n_0}{\partial t} = \frac{\sigma_0}{h\nu} n_0 I - \frac{\sigma_2}{2h\nu} n_0 I^2 + k_S n_S + k_T n_T \quad (1)$$

$$\frac{\partial n_S}{\partial t} = \frac{\sigma_0}{h\nu} n_0 I + \frac{\sigma_2}{2h\nu} n_0 I^2 - (k_S + k_{isc}) n_S - \frac{\sigma_S}{h\nu} n_S I + k_{S2} n_{S2} \quad (2)$$

$$\frac{\partial n_T}{\partial t} = k_{isc} n_S - k_T n_T - \frac{\sigma_T}{h\nu} n_T I + k_{T2} n_{T2} \quad (3)$$

$$\frac{\partial n_{S2}}{\partial t} = \frac{\sigma_S}{h\nu} n_S I - k_{S2} n_{S2} \quad (4)$$

$$n_{T2} = N - n_0 - n_S - n_T - n_{S2} \quad (5)$$

Here, ν is the frequency of the laser radiation, h is the Planck constant, I is the irradiance, and N is the overall number density of chromophore molecules. The constants k_S , k_{S2} , k_T , k_{T2} , and k_{isc} are, respectively, the rate constants for the decays $S_1 \rightarrow S_0$, $S_2 \rightarrow S_1$, $T_1 \rightarrow S_0$, $T_2 \rightarrow T_1$, and $S_1 \rightarrow T_1$. Equations (1) and (2), which reflect the effects of radiative transitions from the ground state, include terms for both single-photon and two-photon $S_0 \rightarrow S_1$ transitions: $\sigma_0 n_0 I [h\nu]^{-1}$ and $\sigma_2 n_0 I^2 [2h\nu]^{-1}$, respectively. At wavelengths at which the linear absorption of the material is non-negligible (here, for wavelengths less than 680 nm), the former process dominates and $\sigma_2(\lambda)$ is set to zero. Conversely, at wavelengths longer than 740 nm, S_1 is assumed to be populated from the ground state primarily by two-photon absorption and $\sigma_0(\lambda)$ is set to zero in the fitting.

Completing the five-band model is the following extinction law, which describes the decrease in intensity of the propagating beam as a result of single-photon absorption from S_1 and T_1 and either single- or two-photon absorption from S_0 , depending on the wavelength.

$$\frac{\partial I}{\partial z} = -(\sigma_0 n_0 + \sigma_S n_S + \sigma_T n_T) I - \frac{\sigma_2}{h\nu} n_0 I^2 \quad (6)$$

Equations (1) through (6) are solved numerically throughout the sample region as described in ref. [25].

Acknowledgements

W.S. acknowledges the financial support from the National Science Foundation (CAREER CHE-0449598) and the Army Research Laboratory (W911NF-06-2-0032).

- [1] a) G. S. He, J. D. Bhawalkar, C. F. Zhao, P. N. Prasad, *Appl. Phys. Lett.* **1995**, *67*, 2433–2435; b) J. E. Ehrlich, X. L. Wu, I. Y. Lee, Z. Y. Hu, H. Pockel, S. R. Marder, J. W. Perry, *Opt. Lett.* **1997**, *22*, 1843–1845.
- [2] a) B. H. Cumpston, S. P. Ananthavel, S. Barlow, D. L. Dyer, J. E. Ehrlich, L. L. Erskine, A. A. Heikal, S. M. Kuebler, I. Y. S. Lee, D. McCord-Maughon, J. Q. Qin, H. Rockel, M. Rumi, X. L. Wu, S. R. Marder, J. W. Perry, *Nature* **1999**, *398*, 51–54; b) S. Kawata, H. B. Sun, T. Tanaka, K. Takada, *Nature* **2001**, *412*, 697–698; c) W. H. Zhou, S. M. Kuebler, K. L. Braun, T. Y. Yu, J. K. Cammack, C. K. Ober, J. W. Perry, S. R. Marder, *Science* **2002**, *296*, 1106–1109.
- [3] a) G. S. He, P. P. Markowicz, T. C. Lin, P. N. Prasad, *Nature* **2002**, *415*, 767–770; b) W. Denk, J. H. Strickler, W. W. Webb, *Science* **1990**, *248*, 73–76; c) B. A. Reinhardt, L. L. Brott, S. J. Clarson, A. G. Dillard, J. C. Bhatt, R. Kannan, L. Yuan, G. S. He, P. N. Prasad, *Chem. Mater.* **1998**, *10*, 1863–1874.
- [4] a) J. D. Bhawalkar, N. D. Kumar, C. F. Zhao, P. N. Prasad, *J. Clin. Laser Med. Surg.* **1997**, *15*, 201–204; b) P. K. Frederiksen, M. Jorgensen, P. R. Ogilby, *J. Am. Chem. Soc.* **2001**, *123*, 1215–1221; c) J. R. Starkey, A. K. Rebane, M. A. Drobizhev, F. Meng, A. Gong, A. Elliott, K. McInerney, C. W. Spangler, *Clin. Cancer Res.* **2008**, *14*, 6564–6573.
- [5] M. Albota, D. Beljonne, J. L. Brédas, J. E. Ehrlich, J. Y. Fu, A. A. Heikal, S. E. Hess, T. Kogej, M. D. Levin, S. R. Marder, D. McCord-Maughon, J. W. Perry, H. Röckel, M. Rumi, G. Subramaniam, W. W. Webb, X. L. Wu, C. Xu, *Science* **1998**, *281*, 1653–1656.
- [6] O. Mongin, L. Porrès, M. Charlot, C. Katan, M. Blanchard-Desce, *Chem. Eur. J.* **2007**, *13*, 1481–1489.
- [7] a) P. Macak, Y. Luo, P. Norman, H. Agren, *J. Chem. Phys.* **2000**, *113*, 7055–7061; b) W. J. Yang, D. Y. Kim, C. H. Kim, M. Y. Jeong, S. K. Lee, S. J. Jeon, B. R. Cho, *Org. Lett.* **2004**, *6*, 1389–1392.
- [8] B. R. Cho, K. H. Son, S. H. Lee, Y. S. Song, Y. K. Lee, S. J. Jeon, J. H. Choi, H. Lee, M. Cho, *J. Am. Chem. Soc.* **2001**, *123*, 10039–10045.
- [9] A. Bhaskar, R. Guda, M. M. Haley, T. Goodson, *J. Am. Chem. Soc.* **2006**, *128*, 13972–13973.
- [10] a) T. K. Ahn, J. H. Kwon, D. Y. Kim, D. W. Cho, D. H. Jeong, S. K. Kim, M. Suzuki, S. Shimizu, A. Osuka, D. Kim, *J. Am. Chem. Soc.* **2005**, *127*, 12856–12861; b) Y. Tanaka, S. Saito, S. Mori, N. Aratani, H. Shinokubo, N. Shibata, Y. Higuchi, Z. S. Yoon, K. S. Kim, S. B. Noh, J. K. Park, D. Kim, A. Osuka, *Angew. Chem.* **2008**, *120*, 693–696; *Angew. Chem. Int. Ed.* **2008**, *47*, 681–684.
- [11] M. Williams-Harry, A. Bhaskar, G. Ramakrishna, T. Goodson, III, M. Imamura, A. Mawatari, K. Nakao, H. Enozawa, T. Nishinaga, M. Iyoda, *J. Am. Chem. Soc.* **2008**, *130*, 3252–3253.
- [12] H. M. Kim, B. R. Cho, *Chem. Commun.* **2009**, 153–164.
- [13] B. J. Coe, M. Samoc, A. Samoc, L. Zhu, Y. Yi, Z. Shuai, *J. Phys. Chem. A* **2007**, *111*, 472–478.
- [14] M. Drobizhev, N. S. Makarov, Y. Stepanenko, A. Rebane, *J. Chem. Phys.* **2006**, *124*, 224701.
- [15] M. K. Kuimova, H. A. Collins, M. Balaz, E. Dahlstedt, J. A. Levitt, N. Sergent, K. Suhling, M. Drobizhev, N. S. Makarov, A. Rebane, H. L. Anderson, D. Phillips, *Org. Biomol. Chem.* **2009**, *7*, 889–896.
- [16] S. Das, A. Nag, D. Goswami, P. K. Bharadwaj, *J. Am. Chem. Soc.* **2006**, *128*, 402–403.
- [17] a) E. Glimsdal, M. Carlsson, B. Eliasson, B. Minaev, M. Lindgren, *J. Phys. Chem. A* **2007**, *111*, 244–250; b) T. J. McKay, J. Staromlynska, P. Wilson, J. R. Davy, *J. Appl. Phys.* **1999**, *85*, 1337–8341; c) J. E. Rogers, J. E. Slagle, D. M. Krein, A. R. Burke, B. C. Hall, A. Fratini, D. G. Mclean, P. A. Fleitz, T. M. Cooper, M. Drobizhev, N. S. Makarov, A. Rebane, K.-Y. Kim, K. S. Schanze, *Inorg. Chem.* **2007**, *46*, 6483–6494; d) C. K. M. Chan, C.-H. Tao, H.-L. Tam, N. Zhu, V. W.-W. Yam, K.-W. Cheah, *Inorg. Chem.* **2009**, *48*, 2855–2864.
- [18] R. Kannan, G. S. He, T. C. Lin, P. N. Prasad, R. A. Vaia, L. S. Tan, *Chem. Mater.* **2004**, *16*, 185–194.
- [19] D. R. McMillin, J. J. Moore, *Coord. Chem. Rev.* **2002**, *229*, 113–121.
- [20] a) K. A. Zachariasse, M. Grobys, Th. von der Haar, A. Hebecker, Yu. V. Il'ichev, Y.-B. Jiang, O. Morawski, W. Kühnle, *J. Photochem. Photobiol. A* **1996**, *102*, 59–70; b) K. A. Zachariasse, M. Grobys, Th. von der Haar, A. Hebecker, Yu. V. Il'ichev, O. Morawski, I. Rückert, W. Kühnle, *J. Photochem. Photobiol. A* **1997**, *105*, 373–383.
- [21] B. Canabate Diaz, S. G. Schulman, A. S. Carretero, F. Gutierrez, *Anal. Chim. Acta* **2003**, *489*, 165–171.
- [22] N. S. Makarov, M. Drobizhev, A. Rebane, *Opt. Express* **2008**, *16*, 4029–4047.
- [23] a) M. Drobizhev, F. Meng, A. Rebane, Y. Stepanenko, E. Nickel, C. W. Spangler, *J. Phys. Chem. B* **2006**, *110*, 9802–9814; b) M. J. Frampton, H. Akdas, A. R. Cowley, J. E. Rogers, J. E. Slagle, P. A. Fleitz, M. Drobizhev, A. Rebane, H. L. Anderson, *Org. Lett.* **2005**, *7*, 5365–5368; c) M. Drobizhev, Y. Stepanenko, Y. Dzenis, A. Karotki, A. Rebane, P. N. Taylor, H. L. Anderson, *J. Am. Chem. Soc.* **2004**, *126*, 15352–15353; d) M. Drobizhev, Y. Stepanenko, Y. Dzenis, A. Karotki, A. Rebane, P. N. Taylor, H. L. Anderson, *J. Phys. Chem. B* **2005**, *109*, 7223–7236.
- [24] M. Sheik-Bahae, A. A. Said, T.-H. Wei, D. J. Hagen, E. W. V. Stryland, *IEEE J. Quantum Electron.* **1990**, *26*, 760–769.
- [25] Y. Li, T. M. Pritchett, J. Huang, M. Ke, P. Shao, W. Sun, *J. Phys. Chem. A* **2008**, *112*, 7200–7207.

- [26] W. Zhang, X. Cao, Z. Hong, Z. Pei, *Org. Lett.* **2005**, *7*, 959–962.
- [27] W. Goodall, K. Wild, K. J. Arm, J. A. G. Williams, *J. Chem. Soc. Perkin Trans. 2* **2002**, 1669–1681.
- [28] K. T. Potts, D. Knowar, *J. Org. Chem.* **1991**, *56*, 4815–4816.
- [29] G. A. Crosby, J. N. Demas, *J. Phys. Chem.* **1971**, *75*, 991–1024.
- [30] J. V. Morris, M. A. Mahaney, J. R. Huber, *J. Phys. Chem.* **1976**, *80*, 969–974.
- [31] J. Van Houten, R. J. Watts, *J. Am. Chem. Soc.* **1976**, *98*, 4853–4858.

Received: May 25, 2010

Revised: October 8, 2010

Published online: January 24, 2011